ELSEVIER

Biochimica et Biophysica Acta 1565 (2002) 168–182

BIOCHIMICA ET BIOPHYSICA ACTA
BBA
www.bba-direct.com

Review

Crystal structure of rhodopsin: a template for cone visual pigments and other G protein-coupled receptors ☆

R.E. Stenkamp[a,b,*], S. Filipek[c], C.A.G.G. Driessen[d], D.C. Teller[e], K. Palczewski[f,g,h]

[a] *Department of Biological Structure, University of Washington, Seattle, WA 98195, USA*
[b] *Biomolecular Structure Center, University of Washington, Seattle, WA 98195, USA*
[c] *Department of Chemistry, University of Warsaw, 1 Pasteur St., PL-02093 Warsaw, Poland*
[d] *Department of Ophthalmology, University of Nijmegen, 6525 EX Nijmegen, The Netherlands*
[e] *Department of Biochemistry, University of Washington, Seattle, WA 98195, USA*
[f] *Department of Ophthalmology, University of Washington, Seattle, WA 98195, USA*
[g] *Department of Pharmacology, University of Washington, Seattle, WA 98195, USA*
[h] *Department of Chemistry, University of Washington, Seattle, WA 98195, USA*

Received 7 December 2001; accepted 16 April 2002

Abstract

The crystal structure of rhodopsin has provided the first three-dimensional molecular model for a G-protein-coupled receptor (GPCR). Alignment of the molecular model from the crystallographic structure with the helical axes seen in cryo-electron microscopic (cryo-EM) studies provides an opportunity to investigate the properties of the molecule as a function of orientation and location within the membrane. In addition, the structure provides a starting point for modeling and rational experimental approaches of the cone pigments, the GPCRs in cone cells responsible for color vision. Homology models of the cone pigments provide a means of understanding the roles of amino acid sequence differences that shift the absorption maximum of the retinal chromophore in the environments of different opsins.

Keywords: Rhodopsin; Retina; Rod photoreceptor; Cone photoreceptor; G-protein-coupled receptor; Vision

1. Introduction

Rhodopsin is a G-protein-coupled receptor (GPCR) that responds to environmental signals, i.e., photons, and initiates intracellular processes that eventually result in an electrical signal processed by the visual system [1–4]. Rhodopsin is an integral membrane protein located in the outer segments of rod photoreceptor cells in the retina [5,6]. Retinas of animals with vision systems capable of wavelength differentiation, i.e., color vision, contain cone cells, the outer segments of which contain opsins as their photoreceptor proteins [7]. Cone opsins have amino acid sequences similar to that of rhodopsin, but with specific differences that affect the wavelength sensitivity of the receptor [8–11].

All opsins contain a retinylidene cofactor covalently bound to the protein via a Schiff-base linkage to a lysine side chain. Absorption of light by the retinal causes a *cis–trans* isomerization of the cofactor. This is followed by a conformational change in the protein that allows binding of a G-protein (transducin) to the cytoplasmic surface of the receptor [12–16]. Rhodopsin is one of the most extensively studied GPCRs. It can be isolated from retina from a number of species. Bovine eyes are readily available from meat packing plants and are a major source of rhodopsin. The presence of the polyene chromophore aids in characterizing and assaying for the protein.

As in the case of other GPCRs, rhodopsin folds into a compact tertiary structure containing seven *trans*-membrane helices [17]. In most cases, GPCRs are located in membrane bilayers with one surface oriented towards the

☆ The homology models for the cone pigments have been deposited in the PDB (identifiers 1KPN, 1KPW and 1KPX).

* Corresponding author. Department of Biological Structure, University of Washington, Box 357420, Seattle, WA 98195-7420, USA. Tel.: +1-206-685-1721.
E-mail address: stenkamp@u.washington.edu (R.E. Stenkamp).

0005-2736/02/$ - see front matter © 2002 Elsevier Science B.V. All rights reserved.
PII: S0005-2736(02)00567-9

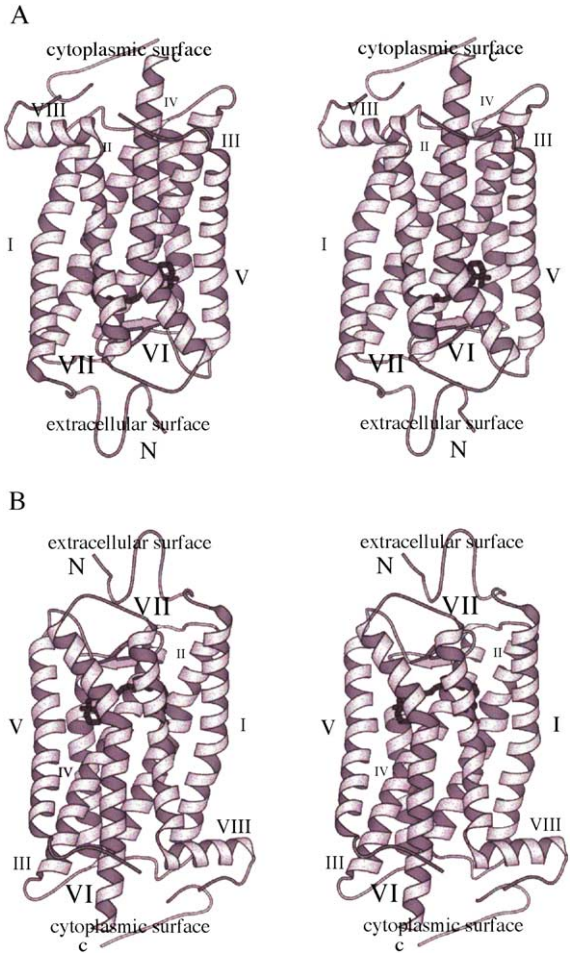

Fig. 1. Stereoviews of rhodopsin. (A) In the orientation favored by vision scientists with the cytosolic surface oriented upwards. (B) In the orientation favored by for other GPCRs with the cytosolic surface facing downwards. In both orientations, the retinal chromophore is shown as a ball-and-stick figure (black) inside the protein. Vertical axis parallel to the membrane normal. Figures drawn with Molscript [55].

cytoplasm of the cell and one towards the extracellular environment. The outer segments of rod cells contain stacks of flattened disks, each of which is a cellular compartment enclosed by a bilayer membrane [7]. Most of the rhodopsin in rod cells is located in these bilayers. Topologically, the intradiscal spaces are equivalent to the extracellular environment sampled by other GPCRs.

GPCRs are a large class of membrane proteins involved in a number of clinically important ligand/receptor processes [18–22]. Accordingly, these proteins are significant drug targets. In most cases, the agonist for these receptors is a small molecule ligand. In the case of rhodopsin, the agonist is the retinal chromophore and a photon. Many GPCRs bind hydrophobic ligands, and comparative studies indicate that the retinal-binding site is similar to the ligand binding sites in other GPCRs [22,23].

The importance of these molecules makes them obvious targets for structural studies, and a number of biophysical techniques have been applied to obtain structural information [12,22,23]. While the seven *trans*-membrane helices could be inferred from sequence analyses and comparisons with bacteriorhodopsin, cryo-electron microscopy (cryo-EM) investigations of rhodopsin provided the first experimental evidence for the seven helices in these molecules [24,25]. A number of spectroscopic techniques have characterized the photostates of the molecule [26,27] and probed the dynamics of the protein as the chromophore and protein conformations change. Spin-label studies have been especially powerful in determining what parts of the structure change in response to photon absorption [28–30]. Also, NMR studies of rhodopsin peptides have characterized the secondary structure of segments of the protein [31], and NMR studies of the complete protein have also been reported [32].

2. Summary of structure determination

Last year, the crystal structure of bovine rhodopsin was obtained at 2.8 Å resolution [33]. A post-doctoral fellow, Dr. T. Okada, developed an efficient protocol for purifying the protein from natural sources [34,35]. The method involves the solubilization of the protein in nonyl glucoside in the presence of 80 mM Zn^{2+}. Under these conditions, other proteins, including bleached rhodopsin and opsin, become insoluble with time and are removed by centrifugation. SDS-PAGE and Western blots of the pellet showed opsin bands. Western blots also identified

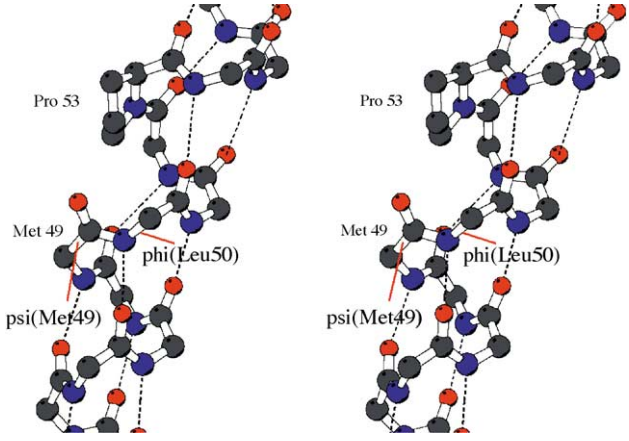

Fig. 2. Stereoview of the kink in helix I. The presence of the proline ring at position 53 and the lack of a hydrogen bond donor for that residue disrupts the structure of the alpha helix. The carbonyl of Met-49 is crowded out of the normal conformation for alpha helical residues. The rest of the helix (beyond Pro-53) bends to accommodate the packing of the proline side chain and this introduces a kink in the helical axis. Figures drawn with Molscript [55].

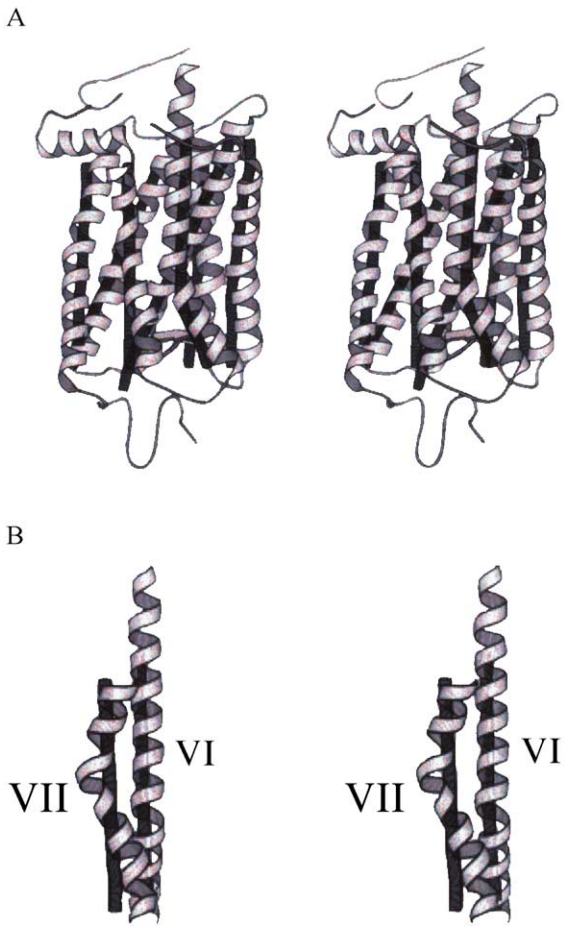

Fig. 3. (A) Stereoview of the rhodopsin structure from the three-dimensional crystals (ribbons) (PDB ident 1HZX) superposed on the helical axes from the two-dimensional cryo-EM study (black rods) [40]. Vertical axis parallel to membrane normal. (B) Stereoview of helices VI and VII after rotation by 90° about the vertical axis. Figures are drawn with Molscript [55].

ion channels, peripherin, ROM, guanylate cyclase and a dehydrogenase. Vapor diffusion crystallization techniques, using ammonium sulfate as the precipitant, yielded diffraction quality crystals [34]. Heptane-1,2,3-triol was used as an additive for crystallization. The crystals were merohedrally twinned and sensitive to visible light. The twinning complicated identification of the correct space group and the initial attempts to solve the structure. Bleaching of the crystals (and concomitant destruction of the diffraction pattern) forced the collection of diffraction data under low levels of red light. Attempts to solve the structure using bacteriorhodopsin as a molecular replacement model failed, so heavy metal derivatives of the natural protein were generated for MIR and MAD phasing experiments. Initial diffraction data for the native protein as well as mercury derivatives were collected at the SSRL and APS synchrotrons, but the structure was solved using a six wavelength mercury MAD data set obtained at SPring8 on a crystal with a 10% twinning ratio. Crystallographic refinement of the two molecules in the asymmetric unit was fairly straightforward [33,36].

3. Protein structure

Fig. 1 shows the resulting structure of rhodopsin with the seven transmembrane helices and the extracellular and cytosolic loops. Fig. 1A shows the molecule in the orientation most familiar to vision scientists with the cytosolic surface facing upwards. Fig. 1B displays the structure in the orientation favored by the GPCR community; extracellular face upwards. The seven transmembrane helices are labeled I through VII, and they span the membrane with the same overall topology as found in bacteriorhodopsin. Helix VIII is a short helix connected directly to helix VII that lies with its helical axis parallel to the membrane surface. The helix most likely does not penetrate deeply into the hydrophobic region of the membrane.

The seven transmembrane helices in rhodopsin are not regular α-helices. The kinks and twists in the helices have been analyzed [37] and in some cases have been associated with elements of 3_{10} or π helix. In helices I, IV, V, VI and VII, the bends are associated with proline residues. Fig. 2 shows the kink in helix I involving Pro-53. While the proline side chain removes the main chain hydrogen bond for this residue, its phi and psi conformational angles are close to those found in α-helices (phi = −49°, psi = −51° in molecule A of Protein Data Bank (PDB) [38] entry 1HZX). The carbonyl of Met-49 would normally make a hydrogen bond to the amide of residue 53, but in this case, it twists away from the helical axis due to close contacts with the proline side chain. The psi angle of Met-49 twists to a slightly lower negative value

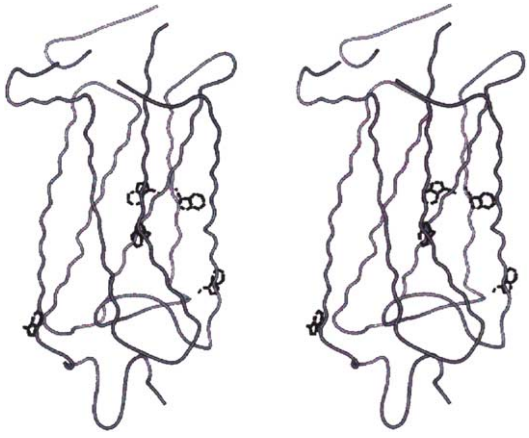

Fig. 4. Stereoview of the backbone tracing of rhodopsin showing the locations of the tryptophan side chains (black ball-and-stick representation). Vertical axis parallel to the membrane normal. Figures are drawn with Molscript [55].

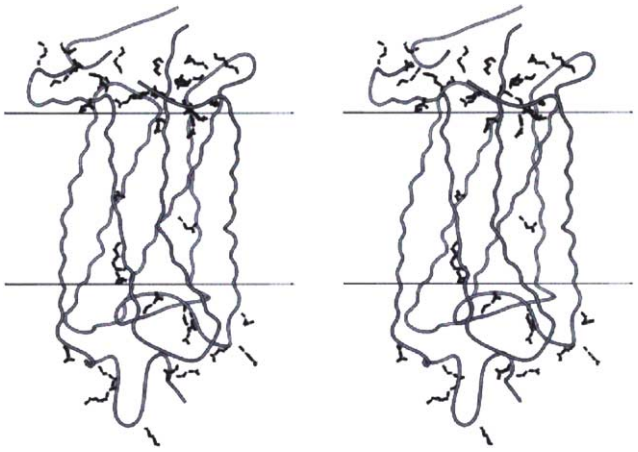

Fig. 5. Stereoview of the backbone tracing of rhodopsin showing the distribution of charged side chains in the molecule. The two horizontal lines denote the surfaces of the membrane bilayer. Vertical axis is parallel to the membrane normal. Figure are drawn with Molscript [55].

than found in alpha helices, $-24°$, and the phi angle of Leu-50 moves to $-112°$. The major conformational changes in the helical residues associated with the inclusion of the proline in the helix occur at residues located one turn towards the N-terminus from the proline.

This same pattern of conformational adjustments occurs at the kink in helix V and the two kinks in helix VII. The bend in helix IV is similar, but it is complicated by the presence of two prolines adjacent to each other in the polypeptide, Pro-170 and Pro-171, and their location near the C-terminal end of the helix. Several more of the residues near the prolines are involved in accommodating the perturbation of the helix by the imino acids.

Helix VI shows the same pattern of conformational adjustments connected with Pro-267, but for this helix, the adjustments in phi and psi occur at residues two and three positions before the proline (Trp-265 and Cys-264). This has the effect of tightening the next turn of the helix, which moves the proline side chain relative to the carbonyl of residue 264 (its normal partner in an alpha helix) and alleviates the close packing of the atoms.

The kink in helix II is not associated with a proline. The helix contains a pair of glycine residues at positions 89 and 90. The helix at this point bulges slightly and accommodates one extra residue with the net effect of introducing a bend in the helix. The phi angle for Gly-90 is $-98°$. Phe-83 has a phi angle of $-83°$, and Phe-91 has a smaller than normal psi angle. A more obvious feature of the distortion is the disruption in the hydrogen bonding pattern that comes with the extra residue. The carbonyl groups of residues 88 and 89 no longer make hydrogen bonds within the helix backbone, nor does the amide of residue 90. It is not obvious what causes these residues to deviate from the normal alpha helical conformation, but it seems likely that the lack of side chain atoms for the glycine residues allows this sort of helix bend.

All of the extracellular loops are visible in our electron density maps, so the molecular model is complete for this surface. Two glycosylation sites are located on this face of the molecule and 11 sugar residues have been added to the model based on the electron density. Two short beta strands are also located on this side of the

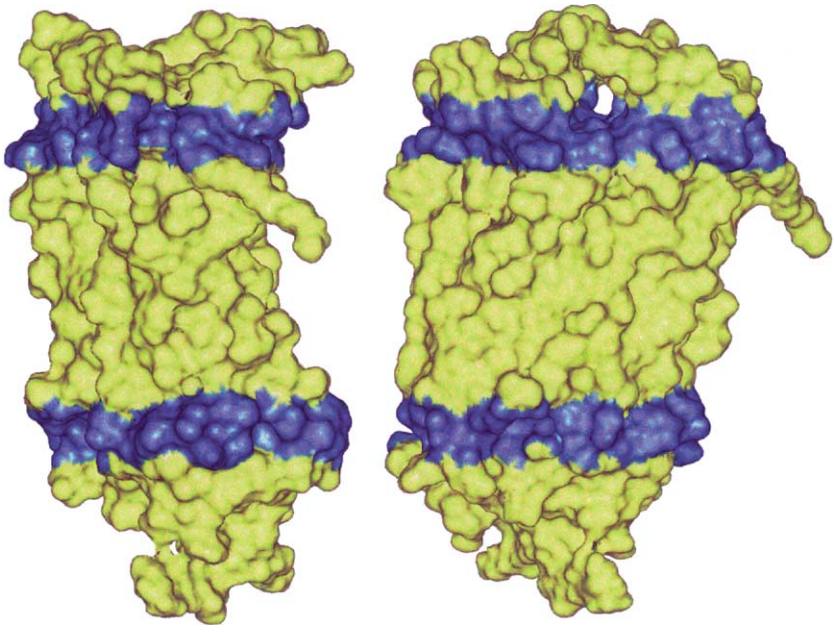

Fig. 6. The molecular surface of rhodopsin in orthogonal views. That part of the surface marking the edges of the membrane bilayer is shown in blue.

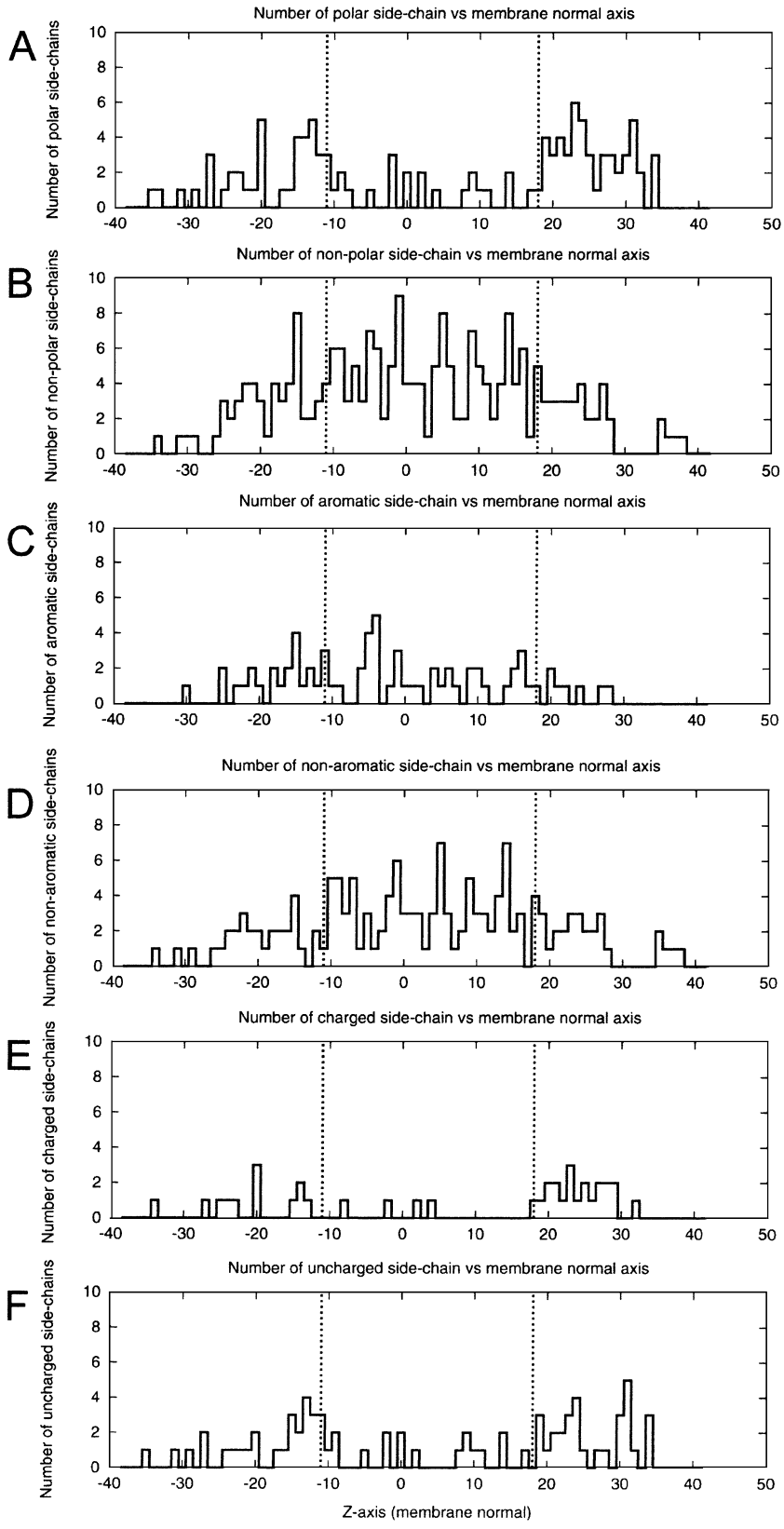

Fig. 7. Distribution of residue types along the direction of the membrane normal. Horizontal scale in angstroms starting on the extracellular side of the protein. The origin on the horizontal scale is taken from the cryo-EM structure [40]. Vertical lines denote margins of the bilayer membrane as identified in Fig. 5. Distributions of: (A) Polar side chains; (B) non-polar side chains; (C) aromatic side chains; (D) non-aromatic, non-polar side chains; (E) charged side chains; (F) uncharged, polar side chains.

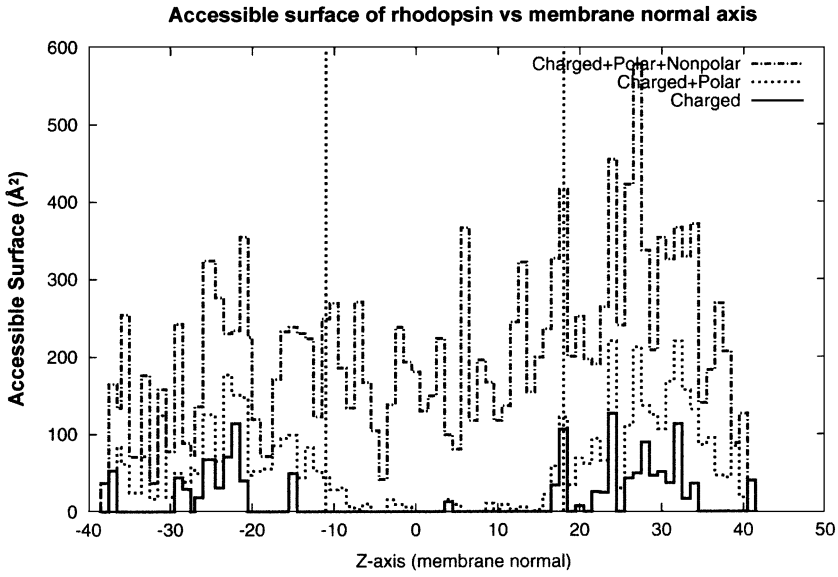

Fig. 8. Distribution of accessible surface area along the direction of the membrane normal. The areas are classified according to the type of atom associated with them. Horizontal axis as in Fig. 7.

transmembrane helices and form a "plug" [39] that limits accessibility to the chromophore site from this surface.

The cytosolic face of the protein is not as well characterized due to static or dynamic disorder of cytoplasmic loop II and the C-terminal tail of the protein. This might be due to defects in the crystal packing in this region, but it is more likely associated with the dynamics of binding of the G-protein to this surface, see below.

4. Comparison with frog rhodopsin

Prior to the crystal structure analysis, cryo-EM studies of frog rhodopsin [25] provided the most detailed view of the molecule. Subsequently, the same group published a low-resolution electron density map showing the arrangement of the seven transmembrane helices in the molecule [40]. Coordinates of the helical axes can be extracted from that map, and Fig. 3A shows the superposition of the molecular model obtained from the three-dimensional crystals on those helical axes. The two structures superpose fairly well and indicate that both structure analyses are free of large experimental or computational artifacts. The structures we are observing are compact, ordered protein structures with seven helices closely packed together.

Cryo-EM and crystallographic techniques show that helix VI is kinked, but they give conflicting views of helix VII. In the bovine rhodopsin structure seen in the three-dimensional crystals, the helix is quite bent and irregular, but in the low resolution structure obtained

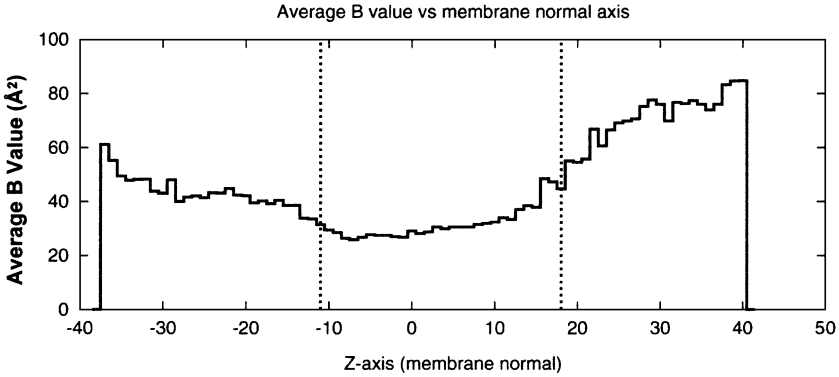

Fig. 9. Average temperature factors along the direction of the membrane normal. Horizontal axis as in Fig. 7.

from two-dimensional crystals, it was interpreted as a straight helix (see Fig. 3B). This modeling difference might be due to the difficulties of interpreting low-resolution electron density maps, or it might be due to chemical differences (photostates) between the frog and bovine rhodopsin preparations.

5. Rhodopsin orientation in the membrane

In addition to confirming the basic structures seen in the two studies, superposition of the bovine rhodopsin structure with that of frog rhodopsin provides the best method for seeing how the molecule is oriented in the membrane. In the cryo-EM study, the *z*-axis of the electron density map is perpendicular to the membrane. In the three-dimensional crystal structure, the two molecules in the asymmetric unit are not oriented in any special direction that gives any information about the alignment of the protein in the membrane. In addition, no intramolecular features provide strong evidence for the location and orientation of the membrane relative to the protein. Thus, alignment of the higher resolution model with the frog rhodopsin helices is the most powerful method for connecting the crystal structure with that in the membrane.

Analyses of amino acid distributions in previous membrane proteins showed that tryptophan side chains are often located at the interface between the bilayers and the aqueous environment [41]. For rhodopsin, that is not the case (see Fig. 4). Only one of the five tryptophans is located near where the protein surface changes from being hydrophobic to being hydrophilic. The other tryptophans are involved in packing interactions between the helices or with the hydrophobic region of the membrane.

Fig. 5 shows the location of charged side chains in rhodopsin. These residues more clearly delimit the hydrophilic and hydrophobic surfaces of the protein. Planes that would exclude most of the charged side chains would be about 30 Å apart. The location of the membrane surfaces is also shown in Fig. 6. This is a reasonable estimate for the membrane thickness, especially since local expansion or contraction of the membrane thickness near the protein is possible. It is interesting that the upper delimiting plane in Fig. 5 lies just at the lower surface of helix VIII. There are a few charged groups between the delimiting planes, notably Lys-296 (site of attachment of the chromophore) and Glu-113 (counterion for the protonated Schiff base). Most of the other internal charged side chains are involved in hydrogen-bonding interactions within the protein, but the side chain of Asp-83 appears to be only weakly involved in those interactions.

Some of the other residue types in rhodopsin are also asymmetrically distributed along the membrane normal. Fig. 7 shows the distribution of residue types. The distributions are as one would expect for a membrane protein. The charged and polar groups tend to be located outside the hydrophobic part of the protein spanning the membrane. Hydrophobic groups, however, are found in the loops between the transmembrane helices as well as along the helices. There is a slight partitioning of the aromatic groups in the protein with more of them associated with the extracellular side of the molecule.

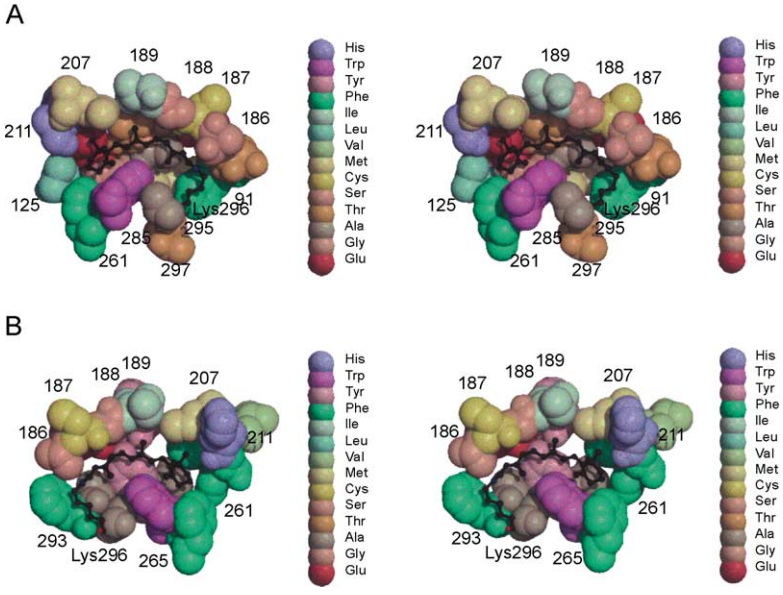

Fig. 10. Stereoviews of the retinal binding site. (A) View of binding site with residues covering the retinal removed. (B) View of binding site after rotation by 180° about the vertical axis. Selected residue numbers are included. Figure drawn with Molscript [55] and Raster3d [56].

This is not reflected in the overall distribution of hydrophobic groups, so the distribution of smaller aliphatic side chains must be shifted to the cytoplasmic side. Perhaps this is associated with the structural flexibility and conformational changes that take place on the cytoplasmic surface in the interactions with G proteins.

Fig. 8 shows the accessible surface along the normal to the membrane plane. The extracellular side is at the negative *z*-axis while the cytoplasmic side is at the positive *z*-axis on the histogram. Three accessible surfaces are plotted: (1) charged atoms, (2) charged and polar atoms, and (3) charged, polar and nonpolar atoms. The last measurement

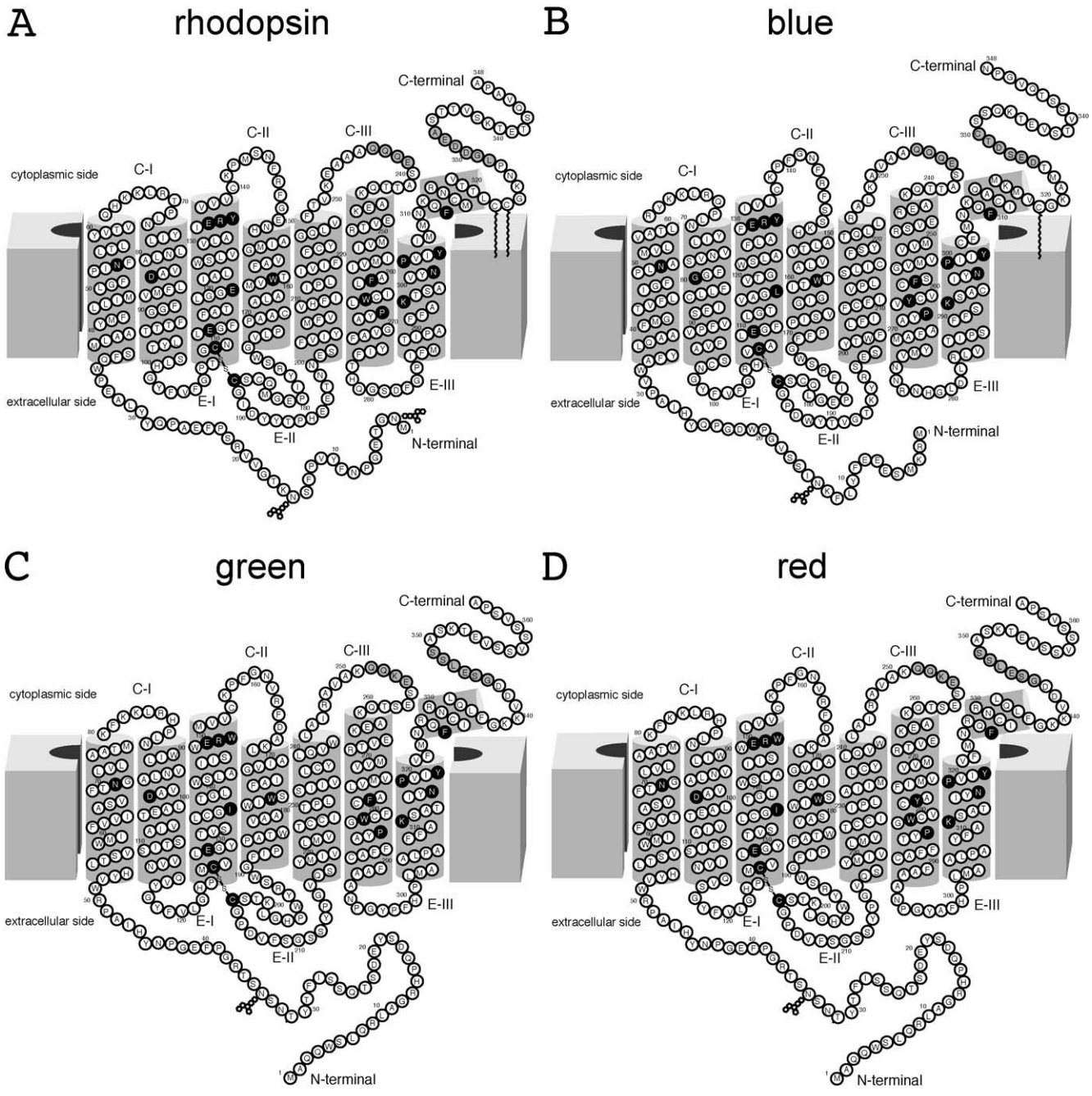

Fig. 11. Two-dimensional models of (A) rhodopsin, (B) blue opsin, (C) green opsin, and (D) red opsin. The transmembrane topology was originally schematically represented by Nathans [57], but it is now improved based on the rhodopsin crystal structure [33]. Key residues are shown in filled circles, while residues not modeled in the rhodopsin crystal structure are marked in grey. Glycosylation sites are denoted by small branched chains on the extracellular side of the protein. Palmitoyl groups are also included near residue 320 for rhodopsin and blue opsin. The extracellular loops are denoted E-I, E-II and E-III. The cytoplasmic loops are C-I, C-II and C-III.

is the total accessible surface for each 1 Å slice. Static accessibility [42] was measured by the method of Shrake and Rupley [43] using the van der Waals radii of Chothia [44].

On the extracellular side of the membrane center, two charged atoms, Glu-201 OE1 and OE2, are accessible to the 1.4 Å probe. This residue is located in the N-terminal region of helix V and nearby electron density has been assigned to a Zn atom with occupancy of 0.5. In the membrane assignment of Teller et al. [36], the residue was placed on the edge of the transmembrane domain, which was postulated to begin at residue 200 in this helix. This residue's alpha carbon position is about 1 Å from what was considered to be the outer edge of the transmembrane domain.

Glu-232 and Arg-252 are the charged residues appearing at 17–20 Å on the *z*-axis coordinate of Fig. 8. Glu-232 is a

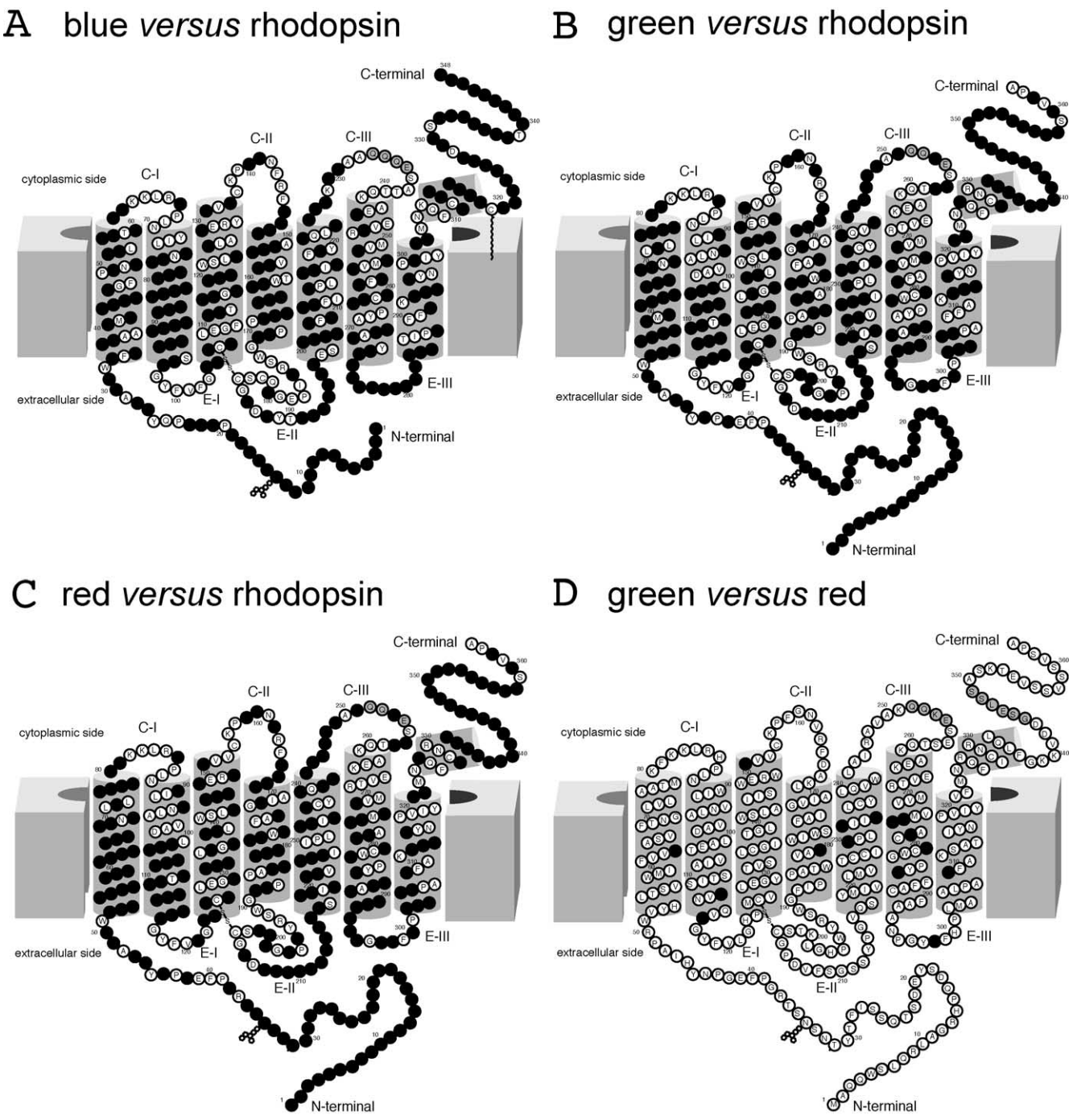

Fig. 12. Two-dimensional models showing amino acid differences between (A) blue opsin and rhodopsin, (B) green opsin and rhodopsin, (C) red opsin and rhodopsin, and (D) green opsin and red opsin. Open circles are identical amino acids in both pigments, while filled circles denote the locations of amino acid differences. The overall homology between the blue, green and red cone pigments versus rhodopsin is 41%, 38% and 37%, respectively.

part of cytoplasmic loop C-III and Arg-252 is located in the N-terminal region of helix VI. These residues are 4 and 6 Å from the inner limit of the transmembrane domain as determined by Teller et al. [36]. The charged portions of these two residues may form a salt bridge, but the position of Glu-232 is uncertain (B factor = 117 Å^2 for its alpha carbon atom). From the coordinates, it looks as if Glu-232 could form a hydrogen bond either with the Arg-252 guanido group or with the Tyr-223 OH by rotation of some chi angles. In the current coordinate set, the guanidinium group of Arg-252 forms a hydrogen bond to O5 of β-nonylglucoside 1501.

The profile of accessible surface of charged and polar atoms resembles the probability density profiles of charged plus polar atoms in the liquid crystallographic structure of a fluid lipid bilayer [45,46]. In the region from $Z = -10$ to $+16$, the accessibility is almost exclusively at nonpolar atoms.

The distribution of average temperature factors along the helix normal is also as expected, see Fig. 9. The center of the molecule is more rigid than the parts outside the membrane. The disorder and flexibility of the cytoplasmic loops and C-terminal tail are consistent with the higher B values on this side of the protein.

6. Retinal binding site

Fig. 10 shows the retinal binding site in rhodopsin. Residues with side chain or main chain atoms within 5 Å are shown in the figure. The chromophore binding site is largely hydrophobic, as would be expected for an environment favorable for a polyene chromophore. Two phenylalanine residues (Phe-212 and Phe-261) are near the ionone ring of the retinal, but Glu-122 also is close to the ring. The side chain of Trp-265 is located near the center of the binding site, and the retinal bends around it in its ground state conformation. Other polar groups near the central part of the polyene are Thr-118 and Tyr-268. Glu-113 is found near the Schiff-base linkage between retinal and Lys-296

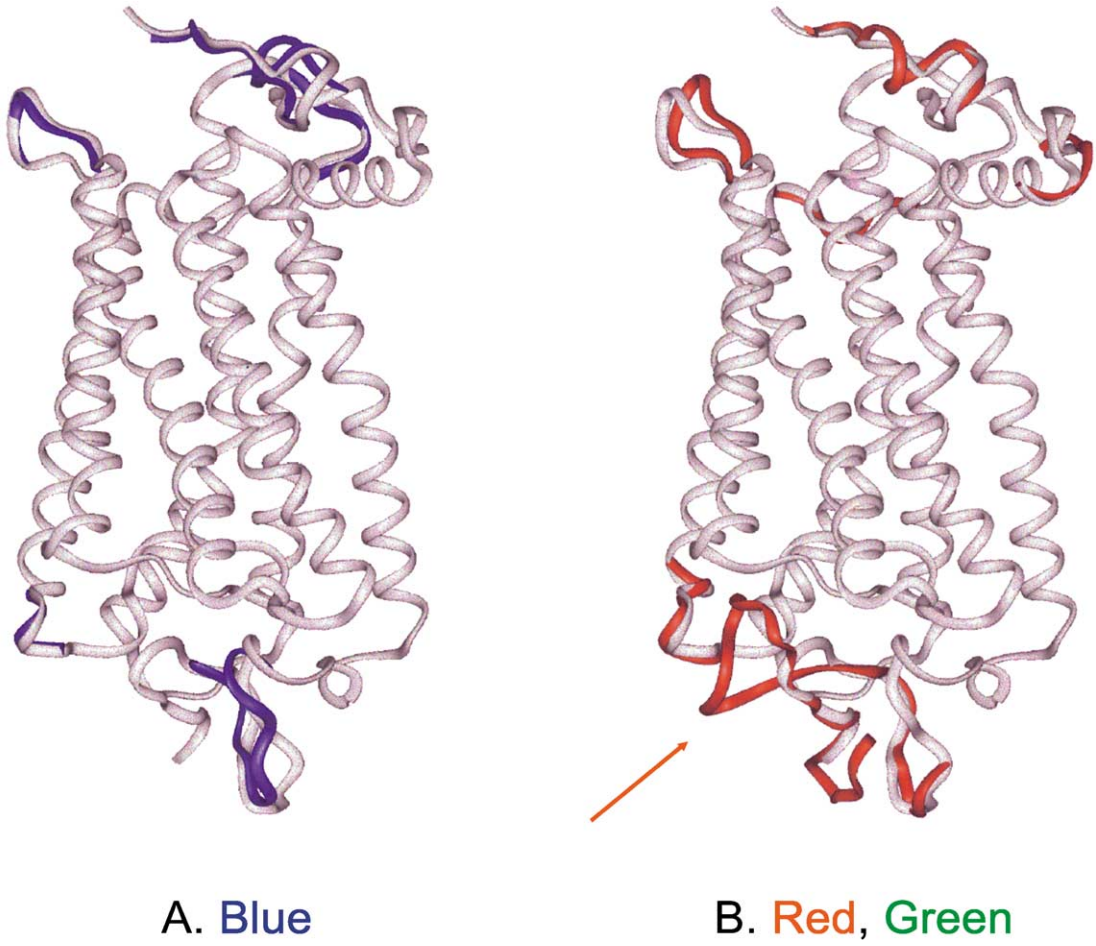

Fig. 13. Superimposition of blue cone pigments and bovine rhodopsin (white). Only major differences between structures are shown for clarity of the picture. (A) Blue cone pigment (in blue). (B) Red and green (the same backbone shown in red). The arrow indicates the location of an additional peptide loop in red and green opsins.

where it can serve as a counterion when the Schiff base is protonated (Fig. 10).

Regeneration of ground state rhodopsin after activation of the protein is associated with removal of the chromophore from the protein, formation of the *cis*-isomer, and reinsertion of the *cis*-conformer into the protein. The crystal structure of the ground state provides no evidence for how the chromophore gains access to the binding site. The site is completely buried and is inaccessible from outside the protein. Accessible surface calculations with smaller probe sizes than the normal 1.4 Å water probe indicate that slight movements of several of the helices would permit access to the site from the hydrophobic center of the bilayer. The binding site accommodates various retinals and their conformations (for recent studies, see Refs. [47,48]).

7. Cone opsins

Cone cells contain photoreceptor proteins related to rhodopsin, but with variations in the residues neighboring the retinal chromophore. The amino acid sequences of the human blue, red and green cone pigments, along with that of bovine rhodopsin, are shown in Fig. 11, superposed on their presumed secondary structure. The amino acid sequence identities for the blue, green and red cone pigments with rhodopsin are 41%, 38% and 37%, respectively. These are shown as differences in Fig. 12. Some of the differences in the amino acid sequences are associated with an altered environment for the chromophore that gives rise to shifts in its absorption spectrum and the wavelength dependence of the receptor's response. Homology modeling of the cone pigments based on the rhodopsin structure provides one means of understanding the molecular basis of color vision.

Theoretical models of cone pigments were constructed with the homology modeling program Modeler [49,50] in the InsightII package. Modeler is a program designed to find the most probable three-dimensional structure of a protein, given its amino acid sequence and its alignment with related structures. The related or reference protein structures are used to derive spatial restraints expressed as probability density functions for each of the restrained features of the model. The individual restraints are assembled into a single molecular probability density function. The 3D protein model is then obtained by an optimization of this probability function. We have used the structure of bovine rhodopsin, 1HZX [36] as a template. To obtain proper alignment of the cone pigment sequences with rhodopsin, we used additional sequences of different GPCR proteins. Limited use was made of the homology-modeling program's restrained simulated annealing molecular dynamics scheme because it was

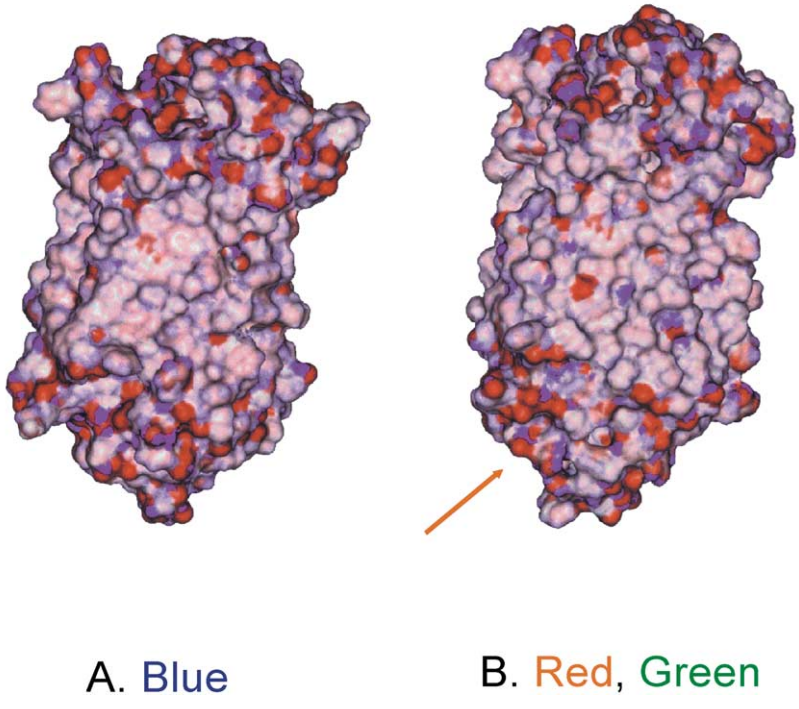

Fig. 14. Surface of cone pigments. Colors denote partial charges of surface atoms. (A) Blue cone pigment. (B) Green (red is very similar). The arrow denotes the location of the additional loop as in Fig. 13. These homology models for the cone pigments have been deposited in the PDB (identifiers 1KPN, 1KPW, 1KPX).

designed for modeling globular proteins while the cone pigments are integral membrane proteins.

To verify whether amino acid sequences of the cone pigments are compatible with the model structure, we used the Profiles-3D program [51] from the InsightII package. The program measures the compatibility of an amino acid sequence with a three-dimensional structure by reducing the structure to a one-dimensional representation, known as a 3D profile, which can be aligned with the sequence. After the homology models were obtained, retinal was inserted into the central cavity and covalently linked to the relevant lysine. The structures of the cone pigments were

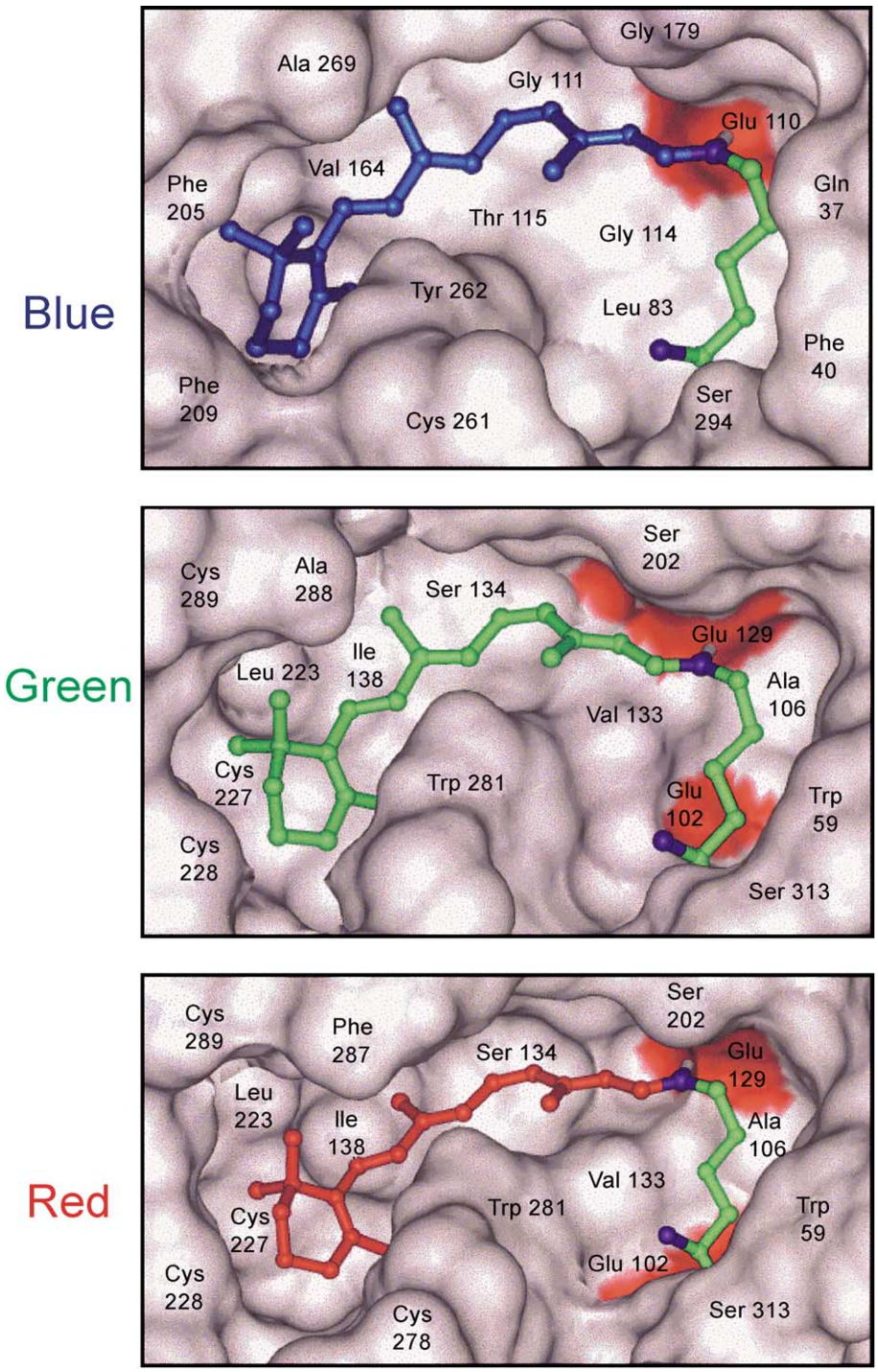

Fig. 15. Vicinity of retinal in cone pigments. Charged amino acids are indicated in red. (A) Blue cone pigment. (B) Green. (C) Red.

subjected to a small degree of optimization confined to a volume within 5 Å of the retinal and covalently linked lysine.

Since the sequences of the cone pigments are closely related to that of rhodopsin, the entire transmembrane region has neither insertions nor deletions in the cone pigment sequences that assist in the homology modeling. Modeler does not require so-called "structurally conserved regions", but instead, it uses all of the sequence and structure information to construct a probability density function. The resulting structures are shown in Fig. 13A for blue and Fig. 13B for red and green cone pigments. Only the major differences between the cone pigments and the template bovine rhodopsin are shown. They are located in the N- and C-terminal regions of the structure. For red and green cone pigments, there is an additional loop of 10 amino acids (indicated with an arrow in Fig. 13B) close to the N-terminal. This loop nicely fits into the rest of the structure so nearly half of the loop is hidden. The sequence alignment of the red and green cone pigments goes beyond the N-terminal so these parts were modeled to maximize interactions with the N-terminal loop. Verification scores from the Profiles-3D program for the models are 103 (red cone pigment) and 106 (green cone pigment). For comparison, the score of bovine rhodopsin 1HZX is 112. For the blue cone pigment, the score is 93. For a protein of this size, a score of 71 or less would indicate a structure that is almost certainly incorrect. These homology models for the cone pigments have been deposited in the PDB (identifiers 1KPN, 1KPW and 1KPX for the blue, green and red cone pigments, respectively).

The secondary structure of all three cone pigments is nearly identical with that of rhodopsin and exhibits seven transmembrane helices, one cytoplasmic helix and two beta strands. The only difference (the same for all cone types) is the extension of the N-terminal beta-strand by one amino acid compared to bovine rhodopsin (results not shown). The surfaces of the cone pigments are similar to the bovine rhodopsin surface (Fig. 14). The partial charges of the surface atoms in the transmembrane domain are close to zero (white color). The cytoplasmic and extracellular domains of the cone pigments contain nearly all the partial charges found on the surface. An arrow denotes, as previously, the additional loop in green and red cone pigments.

Retinal was excluded from the homology modeling process and inserted after the models were built. The vicinity of the retinal in the modeled cone pigments is shown in Fig. 15. As in bovine rhodopsin, the environment around the retinal in all three cone pigments is strongly hydrophobic. Red and green cone pigments share nearly the same sequence so their retinal sites are nearly identical. The central residue forming the cavity is Trp-281 (analogous to Trp-265 in bovine rhodopsin). The counterion to the Schiff base is also glutamic acid, Glu-129 (113 in bovine rhodopsin). There is also another glutamic acid, Glu-102, located near Lys-312, the lysine covalently linked to the retinal. The second glutamic acid probably influences the spectrum by causing a red shift by increasing the negative electron density of the first glutamic acid and hence diminishing the positive charge distribution over the conjugated bonds of retinal. Delocalization of the electrons along the polyene chain is complex and involves stabilization by charged groups including the two glutamates [52,53].

Contrary to other cone pigments, the central residue forming the cavity in blue cone pigments is Tyr-262. Because of the proximity of the retinal beta-ionone ring, Tyr-262 is the major factor in the blue shift of this pigment. The second glutamic acid present in red and green cone pigments is absent in this protein, and this causes an additional blue shift. There are additional residues close to the counterion in all three cone pigments. Ser-183 forms a hydrogen bond with Glu-110 in blue cone pigments (Fig. 16). In green and red cone pigments, there are two serines, 110 and 202, that are able to form a hydrogen bond to the counterion. Whether a hydrogen bond is formed depends on the free energy of this reaction. This is difficult to calculate for such large systems. The existence of chloride ion binding sites in green and red opsins has been postulated [54], and two residues, His and Lys, are believed to be involved in the site. Such a modeled site is shown in Fig. 17. The positive charges of His-197 and additionally Tyr-284 and Ser-202 (and positive charge on the retinal chain) can stabilize Cl^-. In our model, Lys-200 is too far away from the site to interact with Cl^-. These differences between our

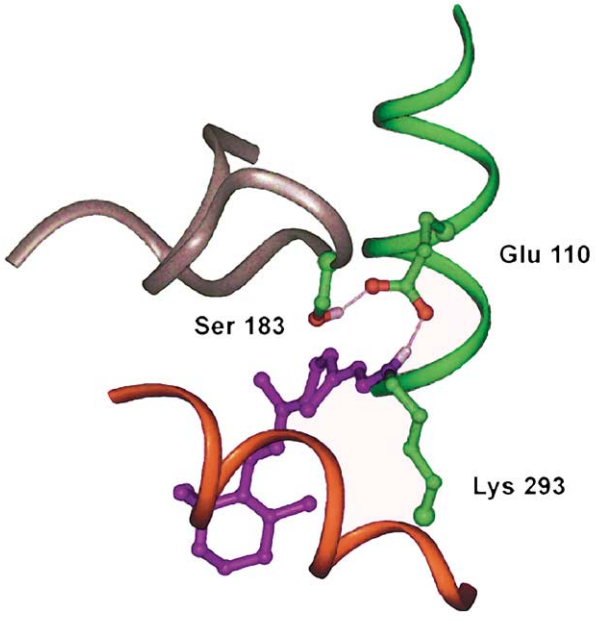

Fig. 16. Influence of Ser-183 on Schiff base interactions in the blue cone pigment.

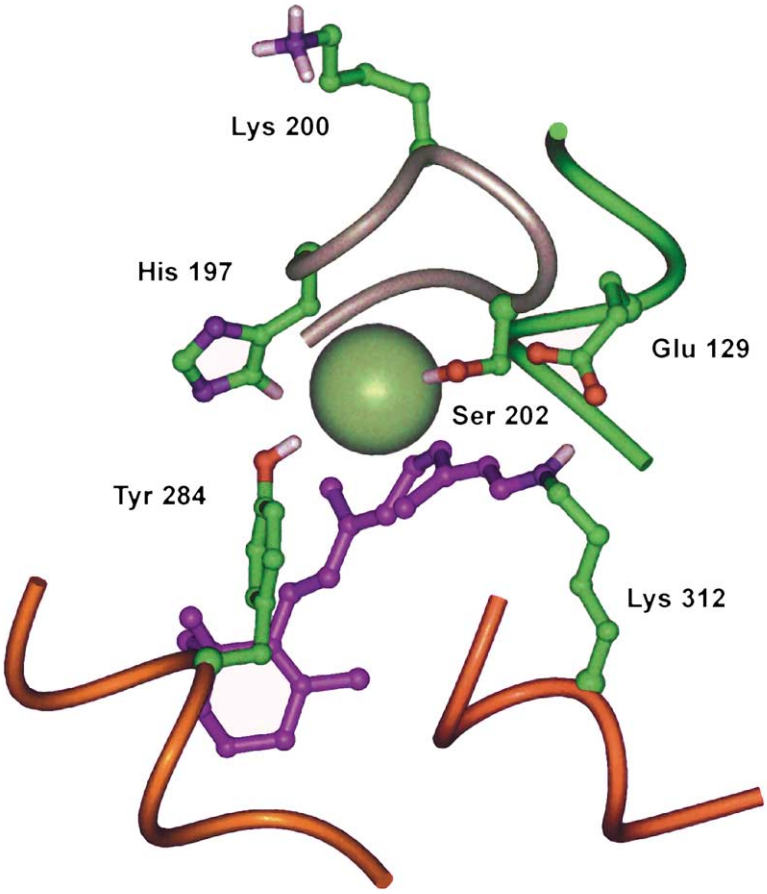

Fig. 17. Model of chloride binding site in green opsin (similar to red opsin).

model and the postulated site [54] could be a result of a long distance effect of the Lys mutants on Cl^- coordination, or the local conformation in this region in our model is not correct. These differences will need to be resolved by further experiments. It is important to mention that these two residues, His and Lys, are strictly conserved in all long-wavelength cone pigments but are absent in all rhodopsins and short-wavelength pigments. The models of the cone pigments contain neither water molecules nor inorganic ions. The influence of these on the spectra is highly dependent on where they are positioned inside the structure and the number of hydrogen bonds they form. Additional calculations are required to elucidate their role in spectral tuning.

Acknowledgements

This research was supported by NIH grants GM63020 and EY08061, a grant from Research to Prevent Blindness (RPB) to the Department of Ophthalmology at the University of Washington, the Alcon Research Institute Award, and the E.K. Bishop Foundation. The computational tasks were partly done in the ICM computer center, University of Warsaw (Poland).

References

[1] Y. Shichida, H. Imai, Cell. Mol. Life Sci. 54 (1998) 1299–1315.
[2] K. Palczewski, Methods Enzymol. 315 (2000).
[3] S. Menon, M. Han, T.P. Sakmar, Physiol. Rev. 81 (2001) 1659–1688.
[4] T. Okada, O.P. Ernst, K. Palczewski, K.P. Hofmann, Trends Biochem. Sci. 26 (2001) 318–324.
[5] P.A. Hargrave, J.H. McDowell, FASEB J. 6 (1992) 2323–2331.
[6] S.T. Menon, M. Han, T.P. Sakmar, Physiol. Rev. 81 (2001) 1659–1688.
[7] J.K. McBee, K. Palczewski, W. Baehr, D.R. Pepperberg, Prog. Retin Eye Res. 20 (2001) 469–529.
[8] J. Nathans, S.L. Merbs, C.H. Sung, C.J. Weitz, Y. Wang, Annu. Rev. Genet. 26 (1992) 403–424.
[9] J. Nathans, C.H. Sung, C.J. Weitz, C.M. Davenport, S.L. Merbs, Y. Wang, Soc. Gen. Physiol. Ser. 47 (1992) 109–131.
[10] J. Nathans, T.P. Piantanida, R.L. Eddy, T.B. Shows, D.S. Hogness, Science 232 (1986) 203–210.
[11] J. Nathans, D. Thomas, D.S. Hogness, Science 232 (1986) 193–202.
[12] T. Okada, O.P. Ernst, K. Palczewski, K.P. Hofmann, Trends Biochem. Sci. 26 (2001) 318–324.

[13] G.L. Fain, H.R. Matthews, M.C. Cornwall, TINS 19 (1996) 502–507.
[14] A. Polans, W. Baehr, K. Palczewski, TINS 19 (1996) 547–554.
[15] H.E. Hamm, Proc. Natl. Acad. Sci. U. S. A. 98 (2001) 4819–4821.
[16] E.C. Meng, H.R. Bourne, TIPS 22 (2001) 587–593.
[17] T. Okada, K. Palczewski, Curr. Opin. Struct. Biol. 11 (2001) 420–426.
[18] M. Vaughan, J. Biol. Chem. 273 (1998) 17297.
[19] T.-H. Ji, M. Grossmann, I. Ji, J. Biol. Chem. 273 (1998) 17299–17302.
[20] U. Gether, B.K. Kobilka, J. Biol. Chem. 273 (1998) 17979–17982.
[21] R.J. Lefkowitz, J. Biol. Chem. 273 (1998) 18677–18680.
[22] J. Ballesteros, K. Palczewski, Curr. Opin. Drug Discov. Dev. 4 (2001) 561–574.
[23] J.A. Ballesteros, L. Shi, J.A. Javitch, Mol. Pharmacol. 60 (2001) 1–19.
[24] G.F.X. Schertler, C. Villa, R. Henderson, Nature 362 (1993) 770–772.
[25] V.M. Unger, P.A. Hargrave, J.M. Baldwin, G.F.X. Schertler, Nature 389 (1997) 203–206.
[26] R.A. Mathies, J. Lugtenburg, Handb. Biol. Phys. 3 (2000) 55–90.
[27] Y. Shichida, H. Imai, Cell. Mol. Life Sci. 54 (1998) 1299–1315.
[28] J.M. Kim, C. Altenbach, R.L. Thurmond, H.G. Khorana, W.L. Hubbell, Proc. Natl. Acad. Sci. U. S. A. 94 (1997) 14273–14278.
[29] A.D. Albert, A. Watts, P. Spooner, G. Groebner, J. Young, P.L. Yeagle, Biochim. Biophys. Acta, Biomembr. 1328 (1997) 74–82.
[30] C. Altenbach, K.W. Cai, H.G. Khorana, W.L. Hubbell, Biochemistry 38 (1999) 7931–7937.
[31] A. Chopra, P.L. Yeagle, J.A. Alderfer, A.D. Albert, Biochim. Biophys. Acta 1463 (2000) 1–5.
[32] P.L. Yeagle, G. Choi, A.D. Albert, Biochemistry 40 (2001) 11932–11937.
[33] K. Palczewski, T. Kumasaka, T. Hori, C.A. Behnke, H. Motoshima, B.A. Fox, I. Le Trong, D.C. Teller, T. Okada, R.E. Stenkamp, M. Yamamoto, M. Miyano, Science 289 (2000) 739–745.
[34] T. Okada, I. Le Trong, B.A. Fox, C.A. Behnke, R.E. Stenkamp, K. Palczewski, J. Struct. Biol. 130 (2000) 73–80.
[35] T. Okada, K. Takeda, T. Kouyama, Photochem. Photobiol. 67 (1998) 495–499.
[36] D.C. Teller, T. Okada, C.A. Behnke, K. Palczewski, R.E. Stenkamp, Biochemistry 40 (2001) 7761–7772.
[37] R.P. Riek, I. Rigoutsos, J. Novotny, R.M. Graham, J. Mol. Biol. 306 (2001) 349–362.
[38] H.M. Berman, J. Westbrook, Z. Feng, G. Gilliland, T.N. Bhat, H. Weissig, I.N. Shindyalov, P.E. Bourne, Nucleic Acids Res. 28 (2000) 235–242.
[39] H.R. Bourne, E.C. Meng, Science 289 (2000) 733–735.
[40] J.M. Baldwin, G.F.X. Schertler, V.M. Unger, J. Mol. Biol. 272 (1997) 144–164.
[41] S.H. White, W.C. Wimley, Annu. Rev. Biophys. Biomol. Struct. 28 (1999) 319–365.
[42] B. Lee, F.M. Richards, J. Mol. Biol. 55 (1971) 379–400.
[43] A. Shrake, J.A. Rupley, J. Mol. Biol. 79 (1973) 351–371.
[44] C. Chothia, Nature 248 (1974) 338–339.
[45] S.H. White, A.S. Ladokhin, S. Jayasinghe, K. Hristova, J. Biol. Chem. 276 (2001) 32395–32398.
[46] K. Hristova, W.C. Wimley, V.K. Mishra, G.M. Anantharamiah, J.P. Segrest, S.H. White, J. Mol. Biol. 290 (1999) 99–117.
[47] G.F. Jang, V. Kuksa, S. Filipek, F. Bartl, E. Ritter, M.H. Gelb, K.P. Hofmann, K. Palczewski, J. Biol. Chem. 276 (2001) 26148–26153.
[48] F.J. Bartl, E. Ritter, K.P. Hofmann, J. Biol. Chem. 276 (2001) 30161–30166.
[49] A. Sali, T.L. Blundell, J. Mol. Biol. 234 (1993) 779–815.
[50] A. Sali, Mol. Med. Today 1 (1995) 270–277.
[51] J.U. Bowie, R. Luthy, D. Eisenberg, Science 253 (1991) 164–170.
[52] M.A. Verhoeven, A.F.L. Creemers, P.H.M. Bovee-Geurts, W.J. de Grip, J. Lugtenburg, H.J.M. de Groot, Biochemistry 40 (2001) 3282–3288.
[53] G.G. Kochendoerfer, S.W. Lin, T.P. Sakmar, R.A. Mathies, Trends Biochem. Sci. 24 (1999) 300–305.
[54] Z. Wang, A.B. Asenjo, D.D. Oprian, Biochemistry 32 (1993) 2125–2130.
[55] P.J. Kraulis, J. Appl. Crystallogr. 24 (1991) 946–950.
[56] E.A. Merritt, D.J. Bacon, Methods Enzymol. 277 (1997) 505–524.
[57] J. Nathans, Biochemistry 29 (1990) 937–942.